Supporting Information

# Gas-templating of hierarchically structured Ni−Co−P for efficient electrocatalytic hydrogen evolution

Peili Zhang[a], Hong Chen[a], Mei Wang[b], Yong Yang[b], Jian Jiang[b], Biaobiao Zhang[a], Lele Duan[a], Quentin Daniel[a], Fusheng Li[a], and Licheng Sun[a,b,*]

[a]*Department of Chemistry, KTH Royal Institute of Technology, Stockholm 10044, Sweden*
[b]*State key Laboratory of Fine Chemicals, DUT-KTH Joint Education and Research Centre on Molecular Devices, Dalian University of Technology, 116023 Dalian, China*
*\*E-mail: lichengs@kth.se*

**Methods**

**The preparation of Ni−P−DF and Co−P−DF**

All chemicals used in the experiments are analytical grade and used as received without further purification. Copper foil with a thickness of 0.025 mm was purchased from Sigma-Aldrich. The foil was cut into $0.5 \times 2$ cm$^2$ pieces and used as substrates. Prior to use, copper foils were washed with acetone, 2 M HCl aqueous solution, and deionized water successively.

The deposition-solution of Ni-P-DF was prepared as follow: Trisodium 2-hydroxypropane-1, 2, 3-tricarboxylate (Sodium citrate tribasic dehydrate, $Na_3(C_6H_5O_7) \cdot 2H_2O$) (20.0 mmol, 6.00 g), ammonium sulfate ($(NH_4)_2SO_4$) (45.0 mmol, 6.00 g) and sodium hypophosphite monohydrate ($Na(H_2O_2P) \cdot H_2O$) (57.0 mmol, 6.00 g) were dissolved in 100 mL water at room temperature. Nickel chloride hexahydrate ($NiCl_2 \cdot 6H_2O$) (14.0 mmol, 3.327 g) were added into the pre-prepared solution with stirring. The pH value of electrodeposition solution was adjusted to 10.0–10.2 by 4.0 M NaOH.

The deposition-solution of Co-P-DF was prepared as follow: Trisodium 2-hydroxypropane-1, 2, 3-tricarboxylate (Sodium citrate tribasic dehydrate, $Na_3(C_6H_5O_7) \cdot 2H_2O$) (20.0 mmol, 6.00 g), ammonium sulfate ($(NH_4)_2SO_4$) (45.0 mmol, 6.00 g) and sodium hypophosphite monohydrate ($Na(H_2O_2P) \cdot H_2O$) (57.0 mmol, 6.00 g) were dissolved in 100 mL water at room temperature. Cobalt nitrate hexahydrate ($Co(NO_3)_2 \cdot 6H_2O$) (14.0 mmol, 4.074 g) were added into the pre-prepared solution with stirring. The pH value of electro deposition solution was adjusted to 10.0–10.2 by 4 M NaOH.
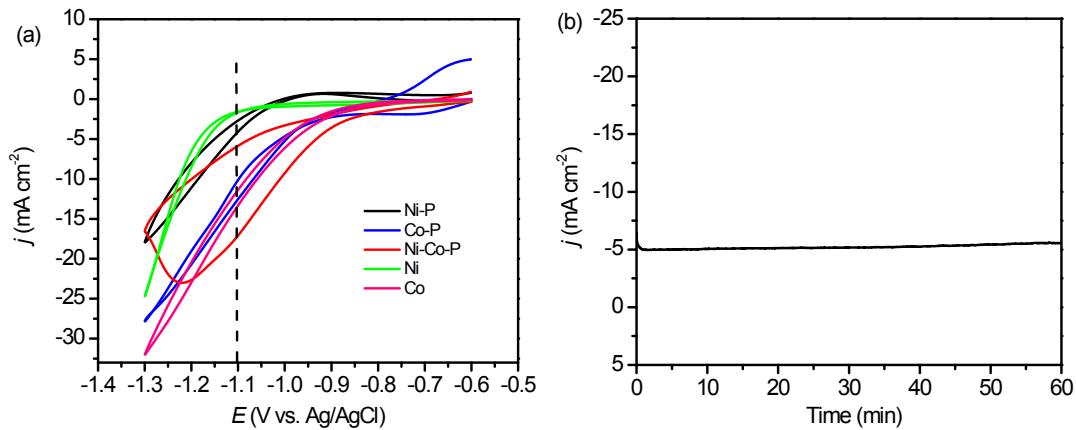
**Fig. S1** (a) Cyclic voltammetry sweeps with copper foil substrates as working electrode in HS-Ni-Co-P, Ni-P-DF, Co-P-DF electrolyte solutions, respectively. (Scan rate: 100 mV s$^{-1}$). $Ni^{2+} + 2\ e^- \rightarrow Ni$, shows a electrodeposition curve (green) with an onset potential of $-1.02$ V vs. Ag/AgCl; $Co^{2+} + 2\ e^- \rightarrow Co$, shows a electrodeposition curve (pink) with an onset potential of $-0.88$ V vs. Ag/AgCl; $Ni^{2+} + (H_2PO_2)^- + 2\ H^+ + 3\ e^- \rightarrow NiP + 2\ H_2O$, shows a electrodeposition curve (black) with an onset potential of $-0.92$ V vs. Ag/AgCl; $2\ Co^{2+} + (H_2PO_2)^- + 2\ H^+ + 5\ e^- \rightarrow Co_2P + 2\ H_2O$, shows a electrodeposition curve (blue) with an onset potential of $-0.89$ V vs. Ag/AgCl. Those results show that $Ni^{2+}$ and $Co^{2+}$ are electrodeposited on the substrate at the same time under $-1.1$ V vs. Ag/AgCl (red). (b) Controlled potential electrodeposition process of the HS-Ni-Co-P film with a copper foil as substrate (applied potential: $-1.1$ V vs. Ag/AgCl).
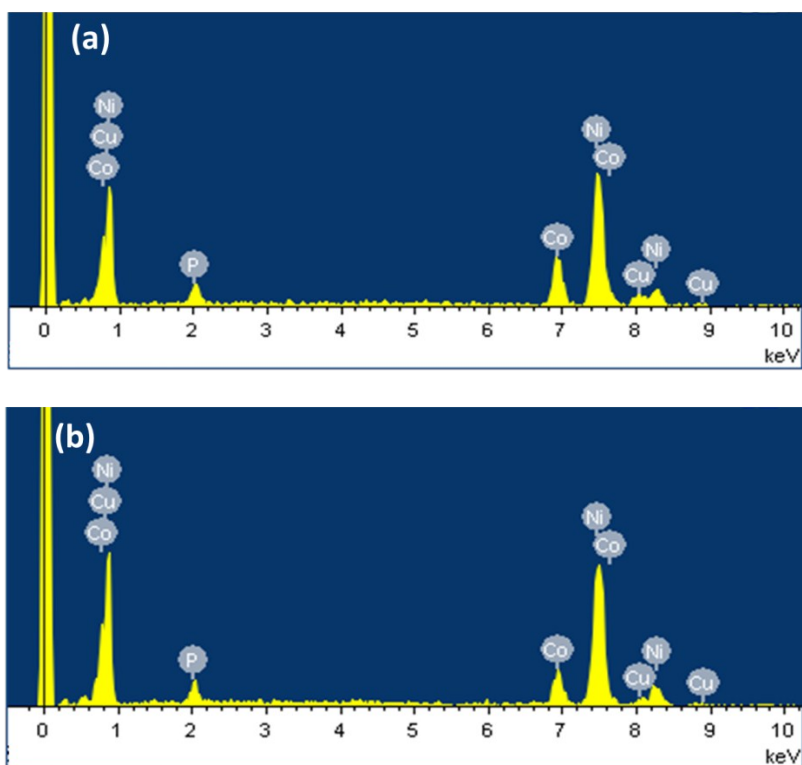
**Fig. S2.** Energy dispersive X-ray spectroscopy (EDS) traces of HS-Ni-Co-P film. (a) EDS of the as-prepared HS-Ni-Co-P film. (b) EDS of the HS-Ni-Co-P after controlled potential electrolysis in 1 M KOH at $\eta = -70$ mV for 50 h.
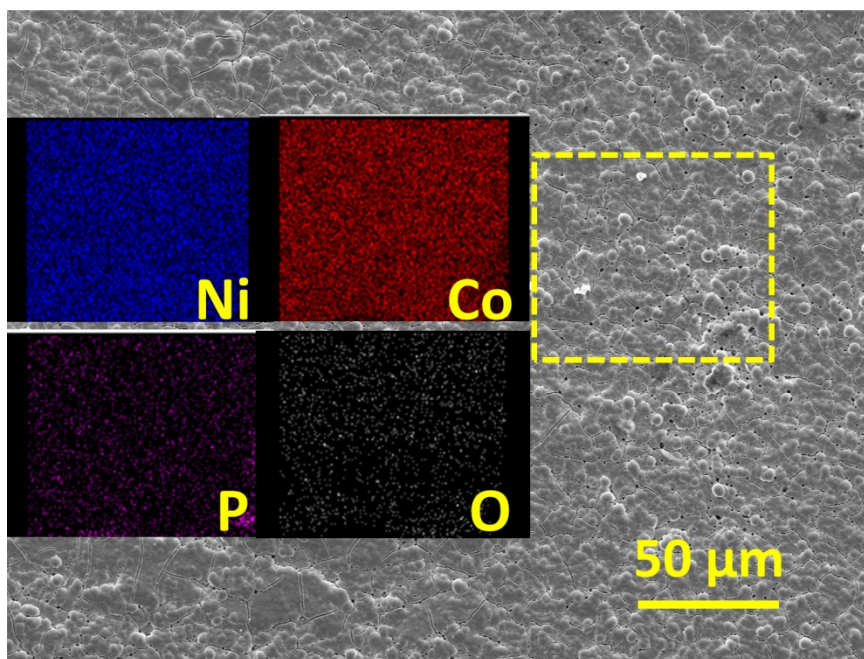


**Fig. S3.** Top-view SEM image and elemental mapping. Top-view SEM image of the HS-Ni-Co-P film and corresponding elemental mapping images.
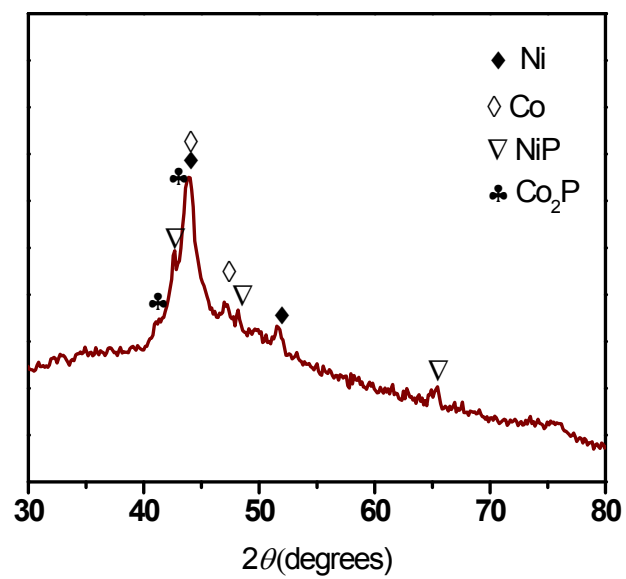
**Fig. S4** Powder X-ray diffraction (PXRD) pattern of the as-prepared HS-Ni-Co-P material.
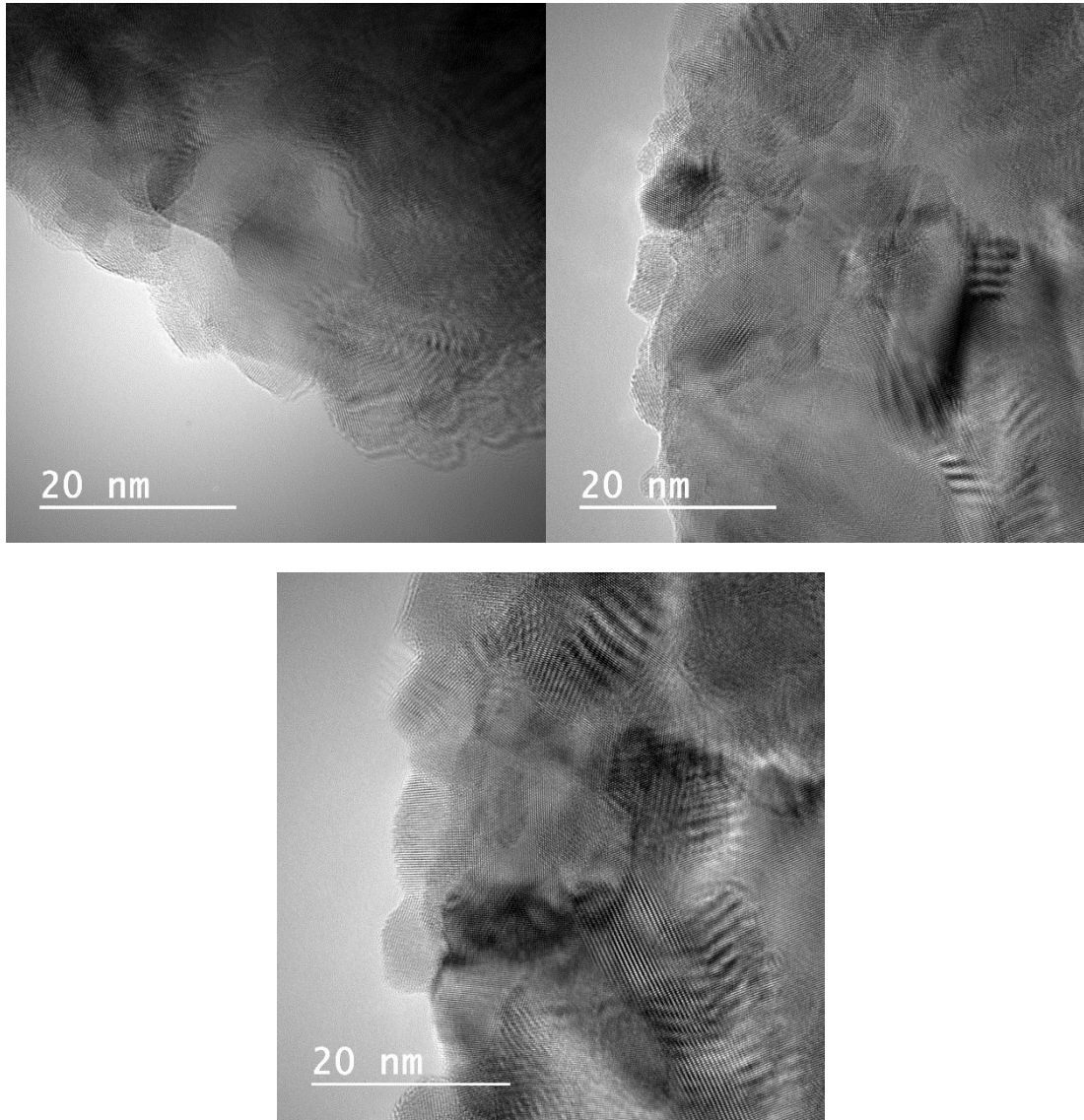
**Fig. S5** TEM images of the as-prepared HS-Ni-Co-P. The observed domain size here is distributed in less than 20 nanometers.
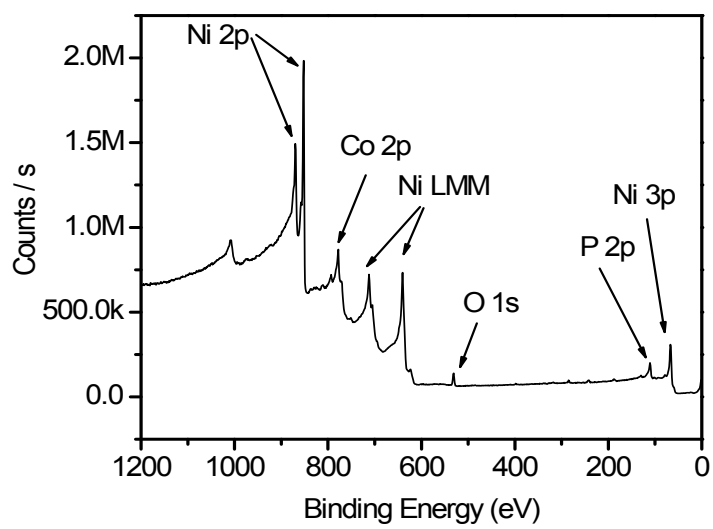
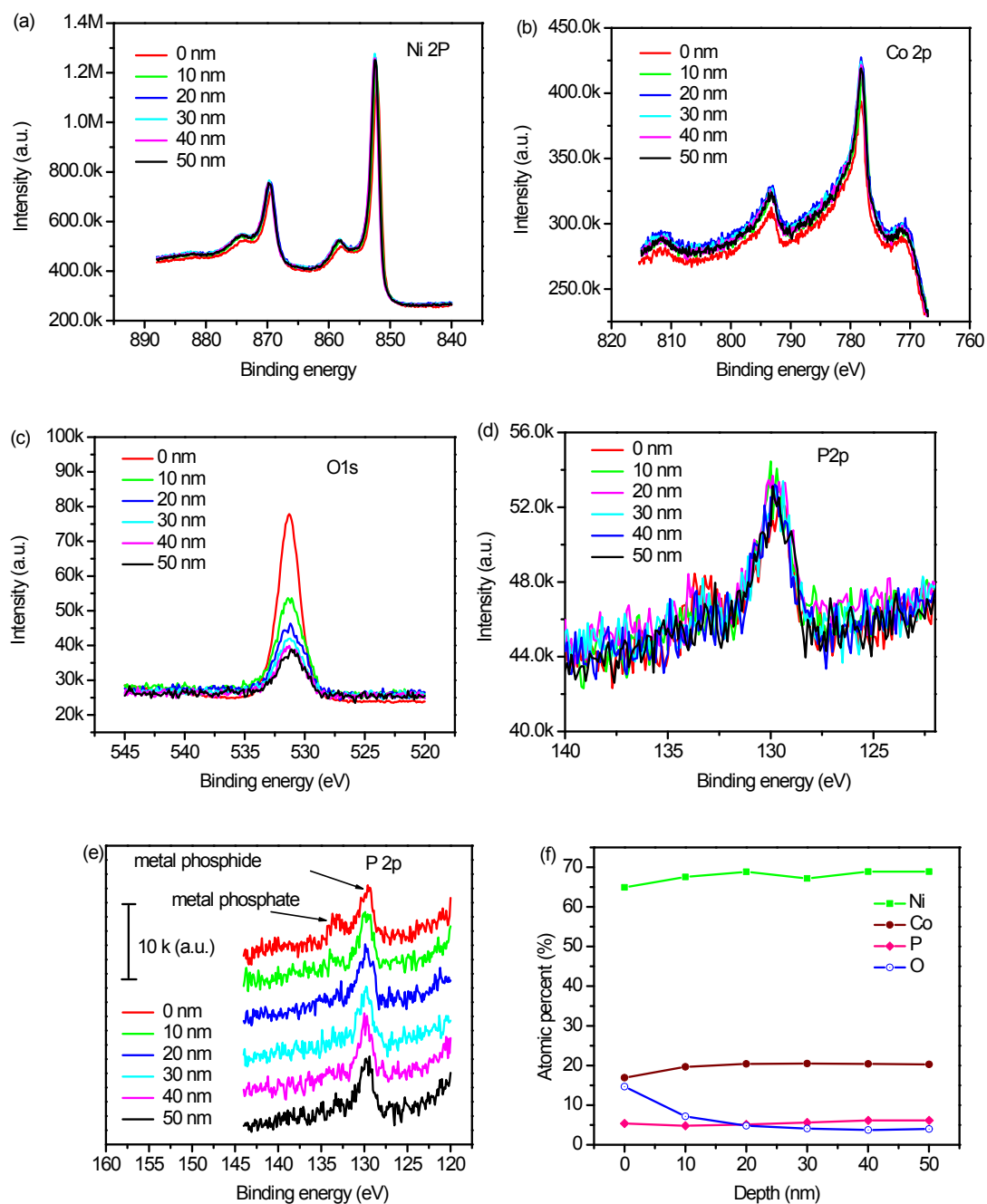**Fig. S6** XPS survey of the as-prepared HS-Ni-Co-P film.

**Fig. S7** Depth profile XPS spectra of the Ni 2p (a), Co 2p (b), O 1s (c) and P 1s (d, e) regions after cycles of argon ion sputtering of HS-Ni-Co-P. The depths are referenced to sputter rates of SiO$_2$. (f) The elemental compositions derived from the spectra in (a), (b), (c) and (d) plotted as a function of sputter depth.
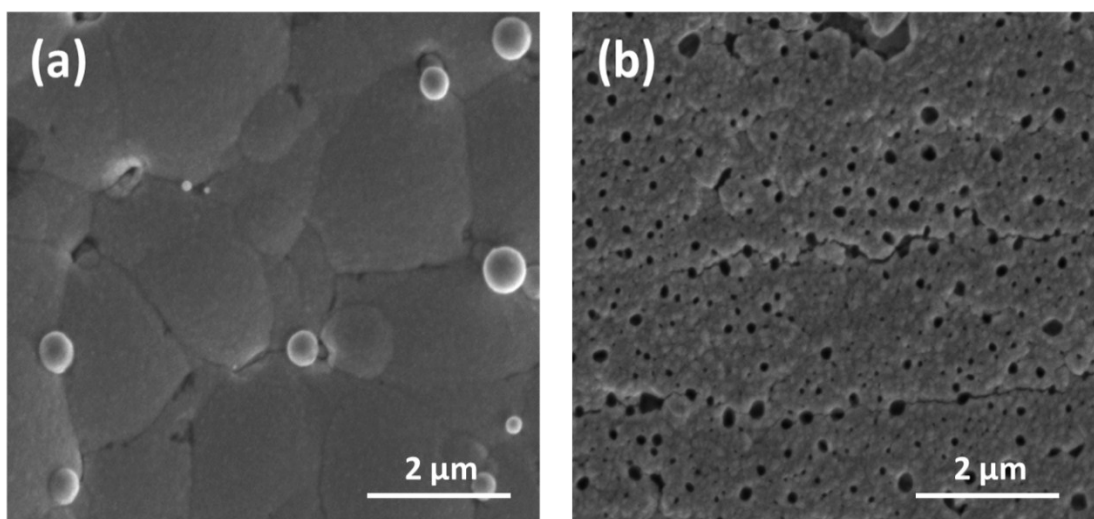
**Fig. S8** Top-view SEM images of the as prepared Ni-P-DF (a) and Co-P-DF (b).
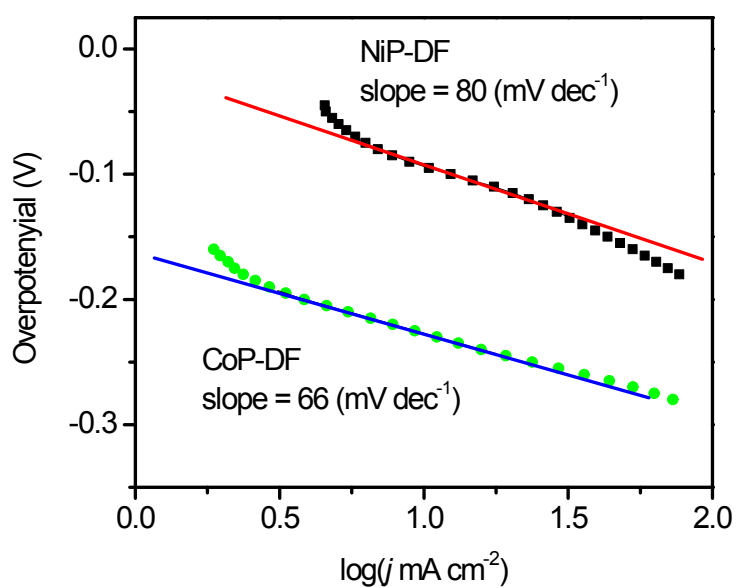


**Fig. S9** Tafel plots for the Ni-P-DF and Co-P-DF catalysts in 1 M KOH aqueous solution.
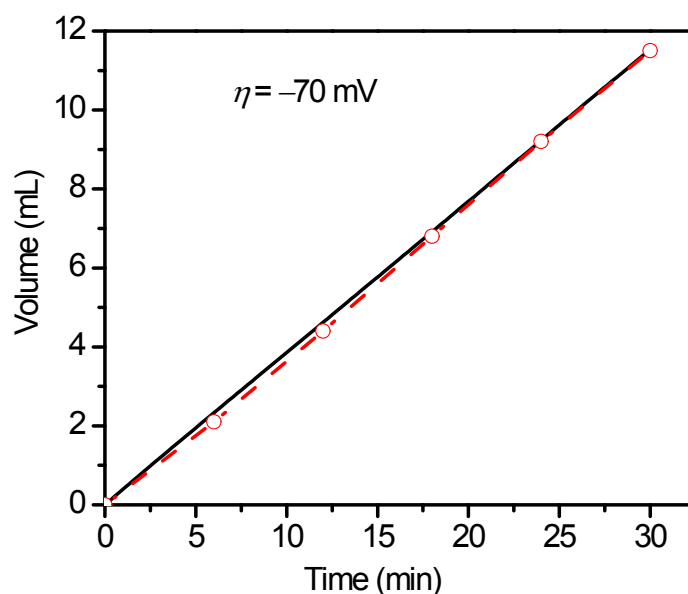
**Fig. S10** Faradaic efficiency of the hydrogen evolution catalyzed by the HS-Ni-Co-P film in 1.0 M KOH aqueous solution at $\eta = -70$ mV. The theoretical line represents the amount of $H_2$ expected for an approximately 100% Faraday efficiency.

**Determination of Faradaic efficiency**

The experiment was performed in a custom built gas-tight electrochemical cell with spheric ground glass joint connected to the automatic sampler system. During controlled-potential coulometry, the gas in the headspace of the cell was analyzed by CEAULIGHT GC-7920 gas chromatograph equipped with a 5 Å molecular sieve column (2 mm × 2 m). The amount of hydrogen evolved was determined by GC with the external standard method and the hydrogen dissolved in the solution was neglected. The amount of hydrogen evolved is in good agreement with that calculated from consumed charge in the CPE experiment (**Fig. S10**), indicating that the HS-Ni-Co-P film operates at a Faradaic efficiency close to 100%.
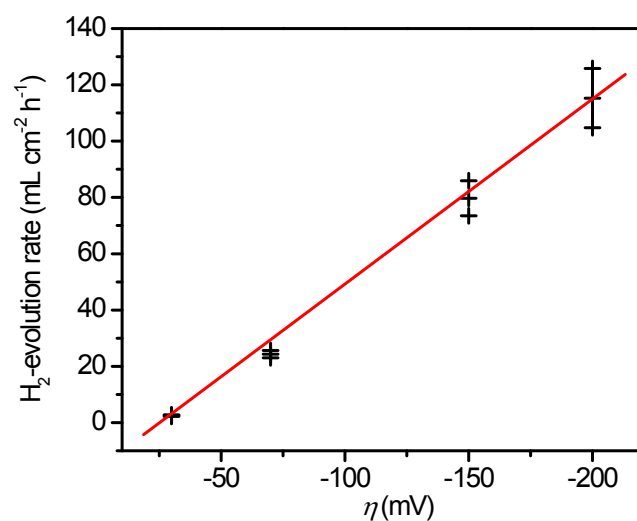
**Fig. S11** H₂ evolution rates of the as-prepared HS-Ni-Co-P film at various applied overpotentials in 1.0 M KOH aqueous solution.
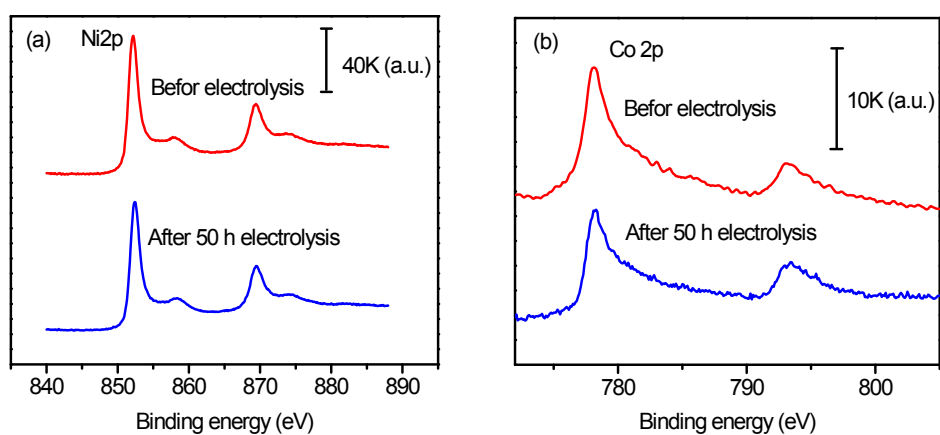


**Fig. S12** Comparison of XPS spectra of (**a**) Ni 2*p* and (**b**) Co 2*p* core level peaks of HS-Ni-Co-P film before and after used for electrolysis in 1.0 M KOH at an overpotential of −70 mV for 50 h.
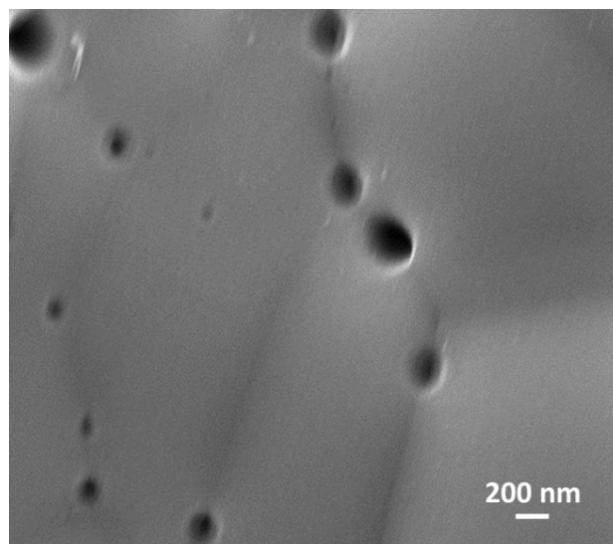
**Fig. S13** SEM image of the HS-Ni-Co-P film after used for the electrolysis in a 1.0 M KOH at an overpotential of −70 mV for 50 h.
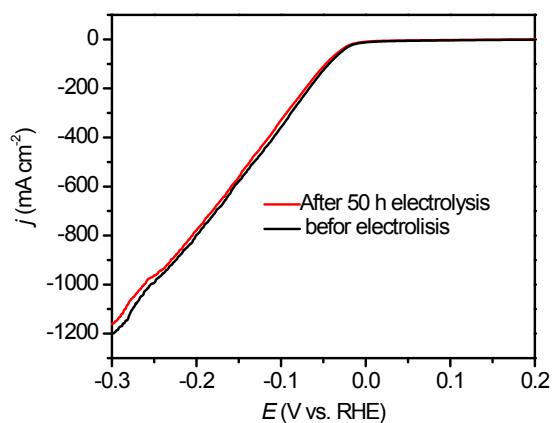


**Fig. S14** LSVs of HS-Ni-Co-P film before and after been used for a 50 h CPE experiment. (conditions: scan rate 5 mV s$^{-1}$, 1.0 M KOH aqueous solution.)
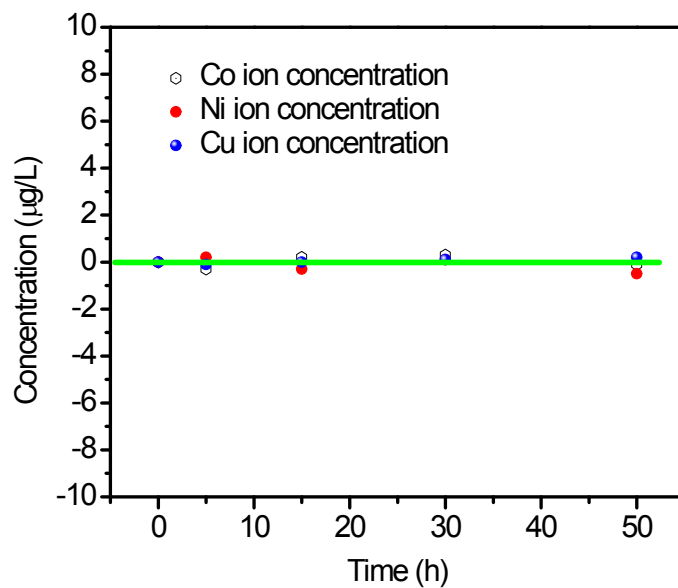
**Fig. S15** ICP-OES analysis. Amount of Ni, Co and Cu ion concentration in the electrolyte during the 50 h CPE analysis at $\eta = -70$ mV with HS-Ni-Co-P as working electrode in 1.0 M KOH.
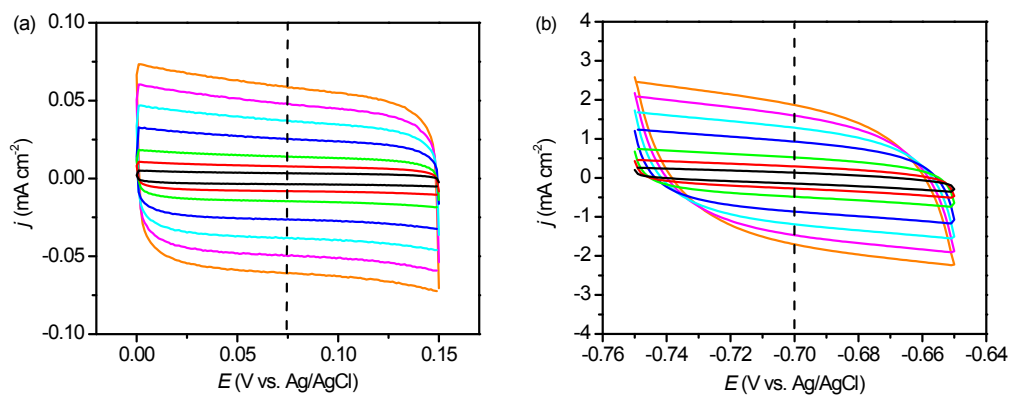
**Fig. S16** Cyclic voltammograms of (a) Pt foil and (b) HS-Ni-Co-P film in 0.3 M KOH aqueous solution, recorded in a Faradaic silence region with varied scan rates from 20 to 500 mV s$^{-1}$.
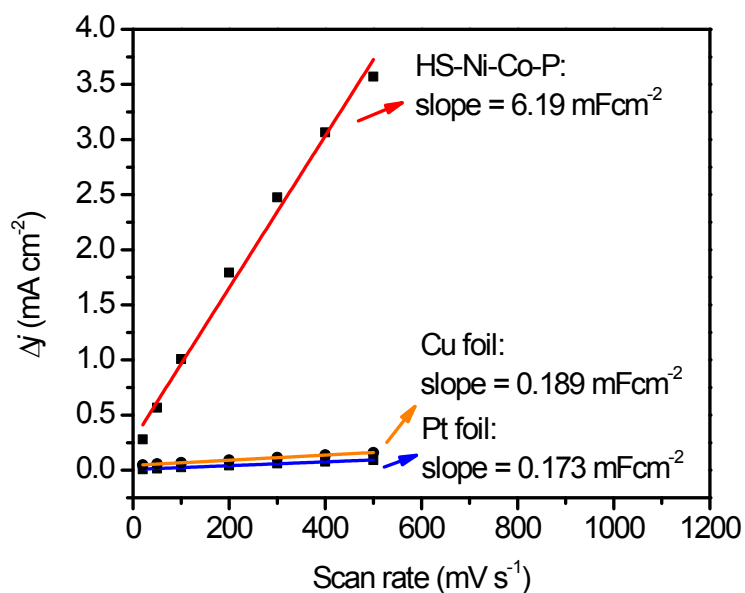


**Fig. S17** Plots of capacitive current as a function of scan rate for the HS-Ni-Co-P film, platinum foil and Cu foil.

**Fig. S18** Plots of capacitive current as a function of scan rate for the HS-Ni-Co-P film, Ni-P-DF film and Co-P-DF film.

**Electrochemical active surface area (ECSA)**

To measure electrochemical capacitance, the potential was swept between 0 to 0.15 V (Platinum foil) or −0.65 to −0.75V (HS-Ni-Co-P, Ni-P-DF and Co-P-DF) versus Ag/AgCl in 0.3 M KOH aqueous solution at each of different scan rates. In these regions, the integrated charge should be due to the charging of the electrode–electrolyte double layer. The capacitive currents 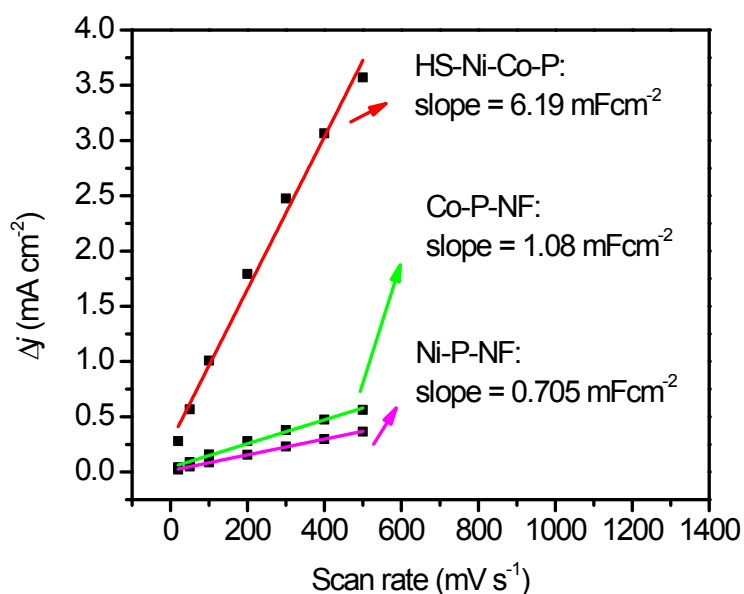were measured at 0.075 V versus Ag/AgCl for Pt foil and at −0.7 V for the as-prepared HS-Ni-Co-P film. The cyclic voltammograms of platinum foil and the as-prepared film are given in Fig. S16. The measured capacitive currents were plotted as a function of scan rate in Fig. S17 and Fig. S18. The specific capacitances were determined to be 6.190 mF cm$^{-2}$ for HS-Ni-Co-P, 0.538 mF cm$^{-2}$ for Co-P-DF, 0.705 mF cm$^{-2}$ for Ni-P-DF, 0.189 mF cm$^{-2}$ for copper foil and 0.173 mF cm$^{-2}$ for platinum foil on the basis of a linear fit. Hence, the ECSA of the catalyst was calculated as: ECSA $= C_{DL}/C_s$. $C_s$ is the specific capacitance and reported to be between 0.022 to 0.130 mF cm$^{-2}$ in alkaline solution. Here, the platinum foil was considered as a flat electrode and used as a control.

$C_{Pt\ foil}/C_s = 0.173$ mF cm$^{-2}/C_s = 1$,

$C_s = 0.173$ mF cm$^{-2}$

For the HS-Ni-Co-P film:

ECSA(HS-Ni-Co-P) = $C_{DL}$(HS-Ni-Co-P)/$C_s$ =6.190/0.173 = 35.9

For the Co-P-DF film:

ECSA(Co-P-DF) = $C_{DL}$(Co-P-DF)/$C_s$ =1.08/0.173 = 6.2

For the Ni-P-DF film:

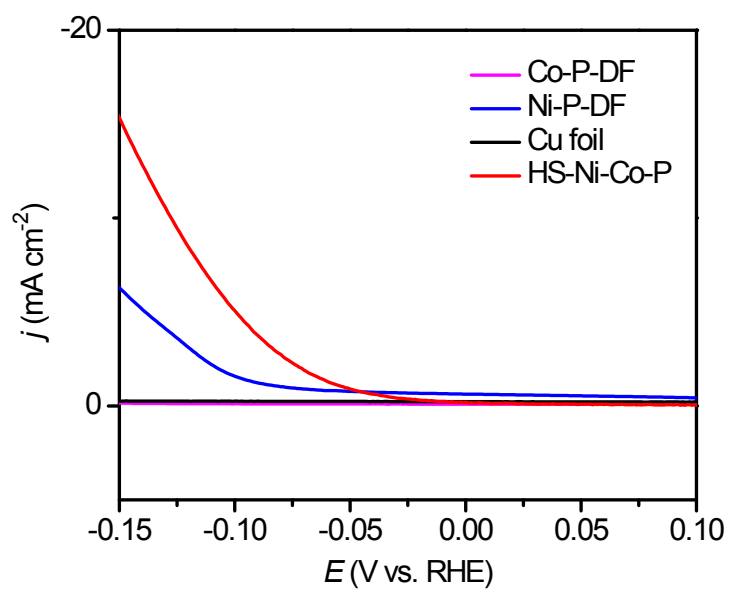ECSA(Ni-P-DF) = $C_{DL}$(Ni-P-DF)/$C_s$ =0.705/0.173 = 4.07



**Fig. S19** Polarization curves of the HS-Ni-Co-P film, Ni-P-DF film, Co-P-DF film, as well as Pt and Cu foil with *j* values normalized by ECSA in 1 M KOH solution.
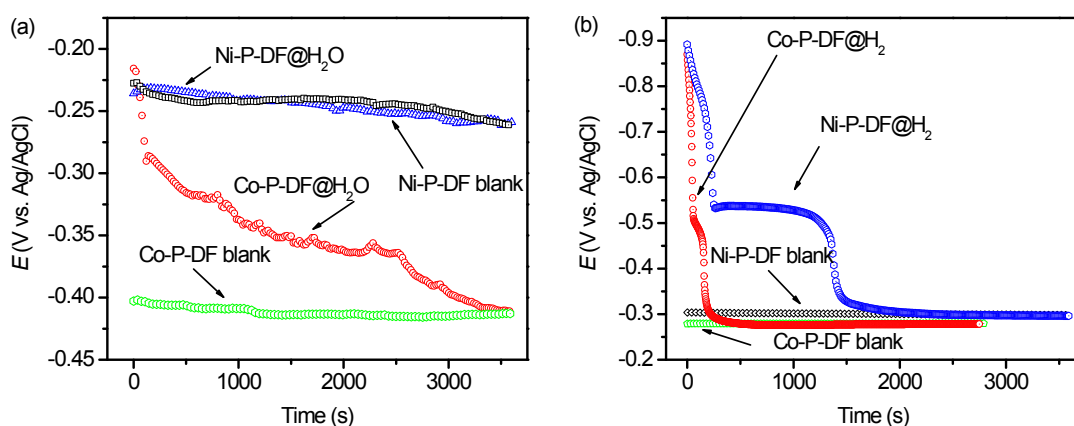
**Fig. S20** Open circuit potential versus time. (a) The $E_{OC}$ versus time curves show the desorption processes of adsorbed $H_2O$ from the Ni-P-DF and Co-P-DF films in acetonitrile solution (0.1 M, $Bu_4NPF_6$) at room temperature. (b) The $E_{OC}$ versus time curves shows the desorption processes of adsorbed $H_2$ from Ni-P-DF and Co-P-DF films in 1.0 M KOH aqueous solution at room temperature.

**Open circuit potential versus time (OCPT) measurements**

The open circuit potential is a parameter which indicates the thermodynamically tendency of a material to electrochemical oxidation in a corrosive medium. After a period of immersion it stabilizes around a stationary value. This potential may vary with time because changes in the nature of the surface of the electrode occur (oxidation, desorption, formation of the passive layer or immunity). The basis of potentiometric concentration measurements is the Nernst equation, which relates the concentration of electroactive species at the electrode surface to the potential at that electrode. Open circuit potential ($E_{OC}$) versus time (OCPT) technique can be used to reveals the desorption properties of $H_2$ and/or $H_2O$ molecules from the working electrode surface. (N.G. Thompson, J.H. Payer, DC Electrochemical Test Methods. Houston. NACE International Ed., 1998)

A conventional three-electrode electrochemical cell was used with a platinum foil (2 × 2 cm$^2$) as counter electrode and an Ag/AgCl electrode as reference electrode. The measurements of OCPT were carried out with a CH instrument 660E potentiostat. The

surface area of the specimen was limited into 0.5 cm$^2$ by epoxy resin before it was immersed in 1.0 M KOH aqueous solution. The electrode surface was assumed as H$_2$ saturated adsorption after been applied at $-1.40$ V vs. Ag/AgCl for 10 s. Vigorous of small H$_2$ bubbles were observed during the process. After short time controlled potential electrolysis, Open circuit potential measurements were carried out immediately. The potential varied with time reveals the desorption process of adsorbed H$_2$ from the electrode surface to the aqueous solution. $T_{dH2}$ was used to represent the period of time for H$_2$ full desorption, from the beginning to the time when the potential equal to the blank. The surface area of the specimen was limited into 0.5 cm$^2$ by epoxy resin before it was immersed in water. The electrode surface was assumed as H$_2$O saturated adsorption after been immersed in water for 15 min. Open circuit potential (OCP) measurements were carried out immediately after the H$_2$O saturated adsorption electrode was fast transfer into the acetonitrile solution (0.1 M, Bu$_4$NPF$_6$). The potential varied with time reveals the desorption process of adsorbed H$_2$O from the electrode surface to the acetonitrile solution. $T_{dH2O}$ was used to represent the period of time for H$_2$O full desorption, from the beginning to the time when the potential equal to the blank.
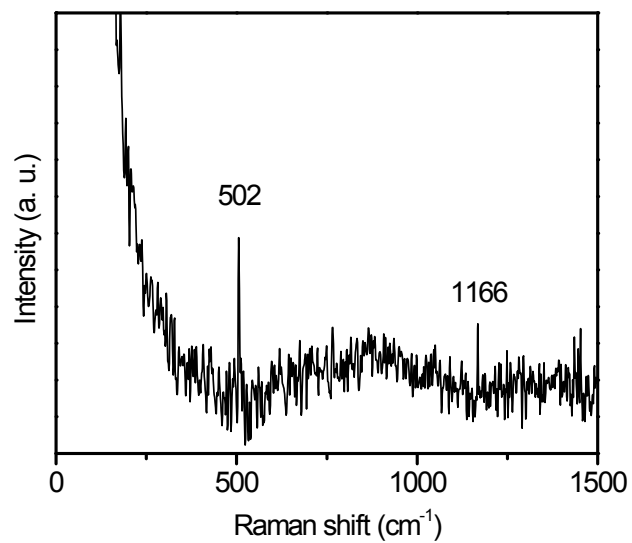
**Fig. S21.** Raman spectra of HS-Ni-Co-P. Two weak absorption peaks at around 503 cm$^{-1}$ and 1166 cm$^{-1}$ can be observed, which arose from the oscillation of cobalt (oxy)hydroxides.
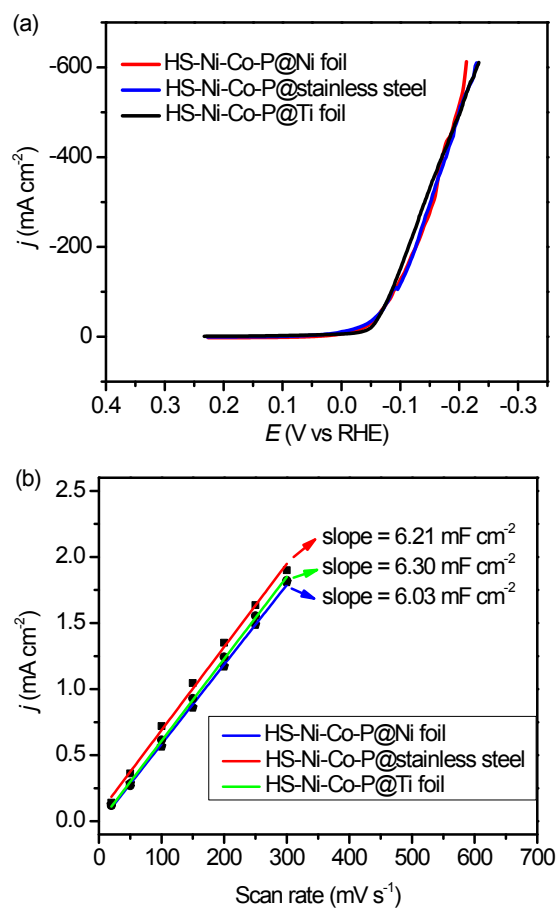
**Fig. S22** (a) HER activities of HS-Ni-Co-P catalysts electrodeposited on various subtrates; (b) Plots of capacitive current as a function of scan rate for the HS-Ni-Co-P film on various subtrates.

**Table S1.** Comparison of selected non-precious HER electrocatalysts in alkaline media.

| Catalysts | Electrolyte | $j$ (mA cm$^{-2}$) | $\eta$ (mV) | Tafel slop (mV dec$^{-1}$) | $j_0$ (mA cm$^{-2}$) | Ref. |
|---|---|---|---|---|---|---|
| HS-Ni-Co-P | 1 M KOH | 10 20 100 500 | 30 49 80 185 | 41 | 1.074 | This work |
| Ni-P-DF | 1 M KOH | 10 | 98 | 80 | 2.453 | This work |
| Co-P-DF | 1 M KOH | 10 | 227 | 66 | 0.145 | This work |
| Ni$_5$P$_4$ | 1 M NaOH | 10 | 49 | 98 | N/A | S1 |
| Ni$_2$P | 1 M NaOH | 10 | 69 | 118 | N/A | S2 |
| NiMo alloy | 2 M KOH | 20 | 70 | N/A | N/A | S3 |
| Co-P film | 1 M KOH | 10 | 94 | 42 | N/A | S4 |
| Co-NRCNTs | 1 M KOH | 10 20 | 370 >450 | N/A | N/A | S5 |
| Co-S/ FTO | 1 M KOH | 1 | 480 | N/A | N/A | S6 |
| FeP NAs/CC | 1 M KOH | 10 | 218 | 146 | N/A | S7 |
| Ni/Ni(OOH)$_2$ | 0.1 M KOH | 10 | >300 | 128 | | S8 |
| MoS$_{2+x}$/FTO | 1 M KOH | 10 | 310 | N/A | N/A | S9 |
| NiB$_{0.54}$ | 1 M KOH | 10 | 135 | 88 | 0.275 | S10 |
| MoB | 1 M KOH | 10 | 200 | 59 | 0.002 | S11 |
| Mo$_2$C | 1 M KOH | 27 | 160 | 54 | 0.004 | S11 |
| CoMnO @CN | 1 M KOH | 28 52 | 100 200 | 152 | N/A | S12 |
| CoOx@CN | 1 M KOH | 10 | 232 | 115 | N/A | S13 |
| NiFeO$_x$ | 1 M KOH | 10 | 88 | N/A | N/A | S14 |
| Ni wire | 1 M NaOH | 10 | 350 | N/A | | S3 |
| NiCo PBA nanocubes | 1 M KOH | 10 | 150 | 60.6 | N/A | S15 |
| Co@N-C | 1 M KOH | 10 | 210 | 108 | N/A | S16 |
| NiFe LDH/NF | 1 M NaOH | 10 | 210 | N/A | N/A | S17 |
| NiCoP nano crystal/nickel foam | 1 M KOH | 10 | 32 | 37 | N/A | S18 |
| np-CuTi alloy | 0.1 M KOH | 10 | 55 | 110 | N/A | S19 |
| Pt/C (wt 48.8%) | 0.1 M KOH | 10 20 | 75 100 | 111 | N/A | S19 |

**References**

[S1] A. B. Laursen, K. R. Patraju, M. J. Whitaker, M. Retuerto, T. Sarkar, N. Yao, K. V. Ramanujachary, M. Greenblatt, G. C. Dismukes, *Energy Environ. Sci.*, 2015, **8**, 1027.

[S2] E. J. Popczun, J. R. McKone, C. G. Read, A. J. Biacchi, A. M. Wiltrout, N. S. Lewis, R. E. Schaak, *J. Am. Chem. Soc.*, 2013, **135**, 9267.

[S3] J. R. McKone, B. F. Sadtler, C. A. Werlang, N. S. Lewis, H. B. Gray, *ACS Catal.*, 2013, **3**, 166.

[S4] N. Jiang, B. You, M. Sheng, Y. Sun, *Angew. Chem. Int. Ed.*, 2015, 54, 6251.

[S5] X. Zou, X. Huang, A. Goswami, R. Silva, B. R. Sathe, R. Mikmeková, T., Asefa, *Angew. Chem. Int. Ed.*, 2014, **53**, 4372.

[S6] Y. Sun, C. Liu, D. C. Grauer, J. Yano, J. R. Long, P. Yang, C. J. Chang, *J. Am. Chem. Soc.*, 2013, **135**, 17699.

[S7] Y. Liang, Q. Liu, A. M. Asiri, X. Sun, Y. Luo, *ACS Catal.*, 2014, **4**, 4065.

[S8] N. Danilovic, R. Subbaraman, D. Strmcnik, K.-C. Chang, A. P. Paulikas, V. R. Stamenkovic, N. M. Markovic, *Angew. Chem. Int. Ed.*, 2012, 51, 12495.

[S9] C. G. Morales-Guio, L. Liardet, M. T. Mayer, M. S. D. Tilley, M. Grtzel, X. Hu, *Angew. Chem. Int. Ed.*, 2015, **54**, 664.

[S10] P. Zhang, M. Wang, Y. Yang, T. Yao, H. Han, L. Sun, *Nano Energy*, 2016, **19**, 98.

[S11] H. Vrubel, X. Hu, *Angew. Chem. Int. Ed.*, 2012, **51**, 12703.

[S12] J. Li, Y. Wang, T. Zhou, H. Zhang, X. Sun, J. Tang, L. Zhang, A. M. Al-Enizi, Z. Yang, G. Zheng, *J. Am. Chem. Soc.* 2015, **137**, 14305.

[S13] H. Jin, J. Wang, D. Su, Z. Wei, Z. Pang, Y. Wang, *J. Am. Chem. Soc.*, 2015, 137, 2688.

[S14] H. Wang, H. W. Lee, Y. Deng, Z. Lu, P.-C. Hsu, Y. Liu, D. Lin, Y. Cui, *Nat. Commun.*, 2015, **6**, 7261.

[S15] Y. Feng, X.-Y. Yu, U. Paik, *Chem. Commun.*, 2016, **52**, 1633.

[S16] J. Wang, D. Gao, G. Wang, S. Miao, H. Wu, J. Li, X. Bao, *J. Mater. Chem. A.*, 2014, 2, 20067.

[S17] J. Luo, J.-H. Im, M. T. Mayer, M. Schreier, M. K. Nazeeruddin, N.-G. Park, S. D. Tilley, H. J. Fan, M. Grätzel, *Science* , 2014, **345**, 1593.

[S18] H. Liang, A. N. Gandi, D. H. Anjum, X. Wang, U. Schwingenschlögl, and H. N. Alshareef, *Nano Lett.*, 2016, **16**, 7718−7725

[S19] Q. Lu, G. S. Hutchings, W. Yu, Y. Zhou, R. V. Forest, R. Tao, J. Rosen, B. T. Yonemoto, Z.

Cao, H. Zheng, J. Q. Xiao, F. Jiao, J. G. Chen, *Nat. Commun.*, 2015, 6, 6567.